Extended Kalman Filter Applied to an AMB System with Strong Magnetic Saturation

Rafal P. Jastrzebski # 1*
LUT Energy, LUT
Lappeenranta, Finland

Alexander Smirnov #2
LUT Energy, LUT
Lappeenranta, Finland

Zongli Lin #3
Univ. of Virginia
Charlottesville, USA

Olli Pyrhönen # 4
LUT Energy, LUT
Lappeenranta, Finland

Paul E. Allaire #5
Univ. of Virginia
Charlottesville, USA

Abstract

The main aim of the paper is to operate an AMB system inside the magnetically saturated region. We investigate how to stabilize a highly nonlinear AMB system with the actuator magnetic saturation by estimating the system states and parameters of the unconstrained bearing in real time. The stabilization is achieved by a combination of the controller and the extended Kalman filter to estimate the states of the plant. In the extended Kalman filter, the magnetization behavior has been modeled by using low-order piecewise polynomial approximation. The extended Kalman applied to the AMB system introduces an additional challenge because of the computational burden, numerical stability when computing the inverse of the innovation covariance matrix, and the non-continuous derivative in the computed Jacobeans. Feasibility of different control configurations is examined. As the case study we use the 1 DOF balancing beam model. The proposed solution for the system operation in the magnetic saturation provides such benefits as: the reduced size and costs of bearings, improved robust performance and stability, and an increased controllability region with respect to control variables.

1 Introduction

In a typical AMB system, the design of the bearings, selection of the operation conditions, and the assumed signal levels are optimized to result in limited and predictable parameter uncertainties. At the same time, such an approach results in an oversized iron part of the bearings to overcome the magnetic saturation of iron and high bias currents to further linearize the magnetic force relation with the position and control currents. The dynamic behavior of the amplifiers can be kept close to the assumed linearized model by limiting the currents and rotor position and by applying such an inner current feedback that prevents the voltage saturation. These design precautions allow more straightforward application of linear control methods, practical control implementation, and increased robust stability of the closed-loop control system.

Complex control algorithms using accurate plant modeling allow robust system behavior despite the nonlinear system dynamics. The extended Kalman filter and its variations provide the common solutions for the estimation of unmeasured system states and unknown system parameters in many applications [1]. However, in AMBs, the relatively fast sampling frequency, typically in the range of 10–40 kHz, poses a challenge for the implementation of the matrix inversion and Jacobian computations for high condition number matrices in real time. Therefore, this subject has not been sufficiently covered in the literature. Modern signal processors and programmable circuits with mature programming tools provide new opportunities for complex AMB control algorithms.

Schuhmann et al. [2] presented the application of the extended Kalman filter for the reduction of noise in the system with collocated capacitive position sensors. In [2], simple nonlinear force without saturation has been considered. Zingerli and Kolar [3] applied a complex nonlinear flux observer with constant observer feedback gain to the inner current-control loop of the cascaded AMB controller.

This paper focuses on the application of the extended Kalman filter to an AMB system with magnetic saturation. The objective is to investigate how to stabilize a highly nonlinear AMB system with the actuator magnetic saturation. The expected result is to use the iron core material beyond the saturation point without losing

*Contact Author Information: rafal.jastrzebski@lut.fi, PL 20, 53851 Lappeenranta, Finland, tel. +358408337618

stability. The observers for the classical current, voltage, and flux control schemes [4] for the measured bearing currents and the angle of the magnetic bearing system are examined.

As a case study, we use a balancing beam model, which is based on the laboratory test rig presented in [5]. The active parts have been redesigned such that the high magnetic saturation of the iron is achieved around the nominal operational point. The relatively simple one-degree of freedom system comprises a straightforward mechanical implementation.

In order to be able to formulate a magnetic force relation of reasonable complexity suitable for the extended Kalman filter implementation, the magnetization behavior has been modeled using a low-order piecewise polynomial approximation. Such a modeling may pose an additional challenge as the non-continuous derivative in the computed Jacobian might result in a solution that is more likely numerically unstable. However, it also simplifies the analytical expressions for system dynamics without compromising the accuracy of the saturation model.

2 Modeling

We select a straightforward LQ control [6] to test with the different AMB control methods and extended Kalman configurations. The plant modeling with magnetic saturation for each described AMB control method is considered. The parameters of the balancing beam model are selected such that the magnetic saturation of the iron core appears for the currents less than the maximum coil current. The parameters of the balancing beam are listed in Appendix A.

2.1 Plant model

Now, the target is to include the magnetic saturation of iron in the dynamical description of the plant. Using Ampere's Circuital Law, assuming a constant magnetic flux density B, and neglecting the stray fluxes and eddy currents, we can approximate the magnetic circuit equation as

$$H_{\mathrm{Fe}} l_{\mathrm{Fe}} + \frac{B}{\mu_0} 2l = Ni \tag{1}$$

where l and i are the air gap (half length of the flux path in the air for horseshoe electromagnet) and the coil current. N is the effective number of coil turns of the AMB stator, H_{Fe} is the magnetic field strength in the iron, and l_{Fe} is the length of the flux path in the iron. We model the BH saturation curve as a first-order piecewise polynomial

$$B = a_k + b_k H_{\mathrm{Fe}}\,, \tag{2}$$

where a_k and b_k are the polynomial coefficients of the saturation model. The flux density and, consequently, the magnetic force of a pair of opposite electromagnets can be obtained by substituting the magnetic field strength from (1) into (2) as

$$B = \mu_0 \frac{l_{\mathrm{Fe}} a_k + b_k N i}{l_{\mathrm{Fe}} \mu_0 + 2 l b_k}, \tag{3}$$

$$f_{\mathrm{m}} = \frac{S_{\mathrm{air}}}{\mu_0}\left(B_2{}^2 - B_1{}^2\right) = \mu_0 S_{\mathrm{air}} \left(\frac{\left(l_{\mathrm{Fe}} a_{2k} + N b_{2k} i_2\right)^2}{\left(l_{\mathrm{Fe}}\mu_0 + 2 b_{2k}\left(l_0 - r\theta\right)\right)^2} - \frac{\left(l_{\mathrm{Fe}} a_{1k} + N b_{1k} i_1\right)^2}{\left(l_{\mathrm{Fe}}\mu_0 + 2 b_{1k}\left(l_0 + r\theta\right)\right)^2} \right). \tag{4}$$

l_0, and r are the average air gap at the zero beam angle θ and the length of the beam arm that is equal to the pivot-to-actuator distance. In each time step, when computing the dynamic model of the plant, a_k and b_k are selected according to the last air gap and coil current for each electromagnet using (1). The applied saturation curve and the saturation as a function of the coil current and the airgap are presented in Figure 1. Assuming infinite relative permeability of iron, the magnetic force f_{m} from (4) simplifies, as a function of bearing currents i_1, i_2, and θ, to

$$f_{\mathrm{m}} = \frac{\mu_0 N^2 S_{\mathrm{air}}}{4} \left(\frac{i_2^2}{\left(l_0 - r\theta\right)^2} - \frac{i_1^2}{\left(l_0 + r\theta\right)^2} \right), \tag{5}$$

Typically, the force relation is linearized in the assumed operational point (l_0, i_0), for example, by applying the bias current i_0 to all the electromagnets and introducing the control current i_c. For the synthesis of the linear controller, (5) becomes

$$f_m = k_i i_c + k_l r\theta \ . \tag{6}$$

The current stiffness k_i and the position stiffness k_l for the set of opposite electromagnets are

$$k_i = \frac{\partial f}{\partial i_c}|_{\theta=0,i_c=0} = \frac{\mu_0 N^2 i_0 S_{air}}{l_0^2} \ , \ k_l = \frac{\partial f}{\partial l}|_{\theta=0,i_c=0} = \frac{\mu_0 N^2 {i_0}^2 S_{air}}{l_0^3} \ . \tag{7}$$

Following Newton's Law, the dynamic equation for the outer position control is

$$J\ddot{\theta} = rf_m. \tag{8}$$

where J is the moment of inertia of the beam.

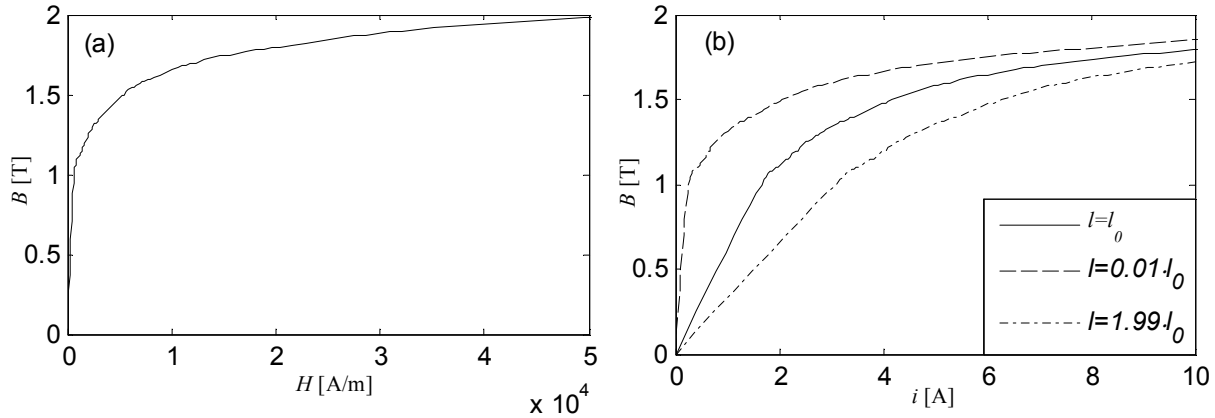

Figure 1: (a) *BH* saturation curve and (b) magnetic flux density as a function of the coil current and airgap

2.1.1 Current Control

This control scheme comprises an inner current control loop, which is often built into the amplifier. In the outer position control, the control current i_c is treated as a state variable. In the current control, it is assumed that the amplifier outputs i_1 and i_2 follow the command reference signals i_{r1} and i_{r2}, where $i_{r2} = (i_0+i_c)$, $i_{r1} = (i_0-i_c)$.

The control inputs are the currents i_1 and i_2 and the measured output is the angle θ. However, the current changes are dependent on the DC link voltage u_{dc} and the internal dynamics of the current amplifiers. The dynamics of the current-controlled amplifier, when neglecting the losses from eddy currents, flux leakage, and magnetic hysteresis, can be described using Ohm's Law and the change in the flux linkage ψ in time

$$u = Ri + \frac{d\psi}{dt} = Ri + \frac{\partial\psi}{\partial i}\frac{di}{dt} + \frac{\partial\psi}{\partial l}\frac{dl}{dt} = Ri + L\frac{di}{dt} + k_u\frac{dl}{dt} = Ri + \frac{\mu_0 S_{air} N^2 b_k}{l_{Fe}\mu_0 + 2lb_k}\frac{di}{dt} - \frac{2N\mu_0 S_{air} b_k \left(l_{Fe}a_k + b_k Ni\right)}{\left(l_{Fe}\mu_0 + 2lb_k\right)^2}\frac{dl}{dt}, \tag{9}$$

where R is the resistance of the coil. In the operational point, when assuming infinite relative permeability of iron, the coil inductance L and the velocity-induced voltage coefficient k_u are

$$L = \frac{\mu_0 S_{\text{air}} N^2}{2l}, \quad k_u = -\frac{\mu_0 N^2 i_0 S_{\text{air}}}{2{l_0}^2} = -\frac{k_i}{2}. \tag{10}$$

The proportional inner current control loops can be modeled as $u=K_c(i_r-i)$. The current gain K_c is selected such that an assumed inner loop bandwidth ω_{bw}=2000 rad/s. Additionally, the voltage saturation can be modeled by substituting the input voltage u as a piecewise polynomial of the reference voltage u_r, for example

$$u = \begin{Bmatrix} u_{\text{r}} & |u_{\text{r}}| < u_{\text{dc}} \\ \text{sig}(u_{\text{r}}) \cdot 0.99 \cdot u_{\text{dc}} + 0.01 \cdot u_{\text{r}} & , |u_{\text{r}}| \geq u_{\text{dc}} \end{Bmatrix}. \tag{11}$$

2.1.2 Voltage Control

The voltage control scheme replaces the above-presented cascaded controller structure with one control loop. In (9) we can see that the voltage, not the coil current, is the actual system input. The joint linearized equations including the voltage-current relation (9), the force-current relation (4), and the equation of motion (8) form the voltage control method. Some discussion about the tradeoffs of the current vs. voltage method can be found, for example, in [7].

An alternative way to present the state equations is to express the magnetic force of a pair of opposite electromagnets using the flux Φ by substituting the flux densities in (4),

$$f_{\text{m}} = \frac{1}{\mu_0 S_{\text{air}}} \left({\Phi_2}^2 - {\Phi_1}^2 \right) \tag{11}$$

The flux can be calculated by integrating the applied voltage u for each electromagnet,

$$\Phi_1 = \frac{1}{N} \int (u_1 - R i_1) dt. \tag{12}$$

The coil currents are among the measured outputs of the plant

$$i_1 = \Phi_1 \frac{2l}{\mu_0 S_{\text{air}} N} + \frac{l_{\text{Fe}}}{\text{N}} \frac{\Phi_1 - a_k S_{\text{air}}}{b_k S_{\text{air}}}. \tag{13}$$

2.1.3 Flux Control

As a third alternative, the flux control scheme can be applied [4]. However, instead of using the flux measurement as in [4], we apply the estimated flux from the measured currents [3,8]. In this case, the outer position controller provides the reference force signal f_r to the inner flux controllers. In the inner controller, the reference force can be changed to the reference flux

$$\Phi_{\text{r}} = \sqrt{f_{\text{r}} \mu_0 S_{\text{air}}}. \tag{14}$$

In the basic case, the proportional current feedback is replaced with the flux feedback control $u_r = K_\Phi(\Phi_r-\Phi_{es})$, where the feedback gain K_Φ is selected analogically to the current feedback gain K_c. The estimated flux Φ_{es} is computed using the flux observer

$$\frac{d\Phi_{\text{es}}}{dt} = \frac{1}{N}(u_{\text{r}} - R i_{\text{es}}) - L_{\text{ob}}(i_{\text{es}} - i), \; i_{\text{es}} = \Phi_{\text{es}} \frac{2l}{N S_{\text{air}} \mu_0} + \frac{l_{\text{Fe}}}{N} \frac{\Phi_1 - a_k S_{\text{air}}}{b_k S_{\text{air}}}. \tag{15}$$

Now, the position controller is not dependent on the magnetic force nonlinearities. Therefore, the implementation of the extended Kalman filter (EKF) can be considered for the flux observers in the inner control loops.

2.2 Extended Kalman Filter

The EKF is a nonlinear version of the popular Kalman filter that uses current mean and covariance estimates as a linearization point. We consider a nonlinear discrete-time stochastically disturbed process model with Gaussian uncorrelated noise processes $\mathbf{w}_k$ and $\mathbf{v}_k$ described by

$$\mathbf{x}_{k|k-1} = f\left(\mathbf{x}_{k-1|k-1}, \mathbf{u}_{k-1}\right) + \mathbf{w}_{k-1}, \quad \mathbf{y}_{k-1} = g\left(\mathbf{x}_{k-1|k-1}\right) + \mathbf{v}_k, \tag{16}$$

where $\mathbf{x}$ and $\mathbf{y}$ are the state vector and the output vector, respectively. We use the discrete-time formulation as follows [9, 10]. First, the discrete prediction state estimate $\hat{\mathbf{x}}$ and the output estimate $\hat{\mathbf{y}}$ of the nonlinear plant together with the Jacobian matrices are computed

$$\hat{\mathbf{x}}_{k|k-1} = f\left(\hat{\mathbf{x}}_{k-1|k-1}, \mathbf{u}_{k-1}\right), \quad \hat{\mathbf{y}}_{k-1} = g\left(\hat{\mathbf{x}}_{k-1|k-1}\right), \quad \mathbf{F}_{k-1} = \left.\frac{\partial f}{\partial x}\right|_{\hat{\mathbf{x}}_{k-1|k-1}, \mathbf{u}_{k-1}}, \quad \mathbf{C}_k = \left.\frac{\partial g}{\partial x}\right|_{\hat{\mathbf{x}}_{k|k-1}}, \tag{17}$$

where $\mathbf{u}$ is the vector of control inputs that are currents or voltages depending on the control method. The subscript $k|k$-1 denotes the estimation at the time step k with the measurement from the time step k+1. Next, we compute the covariance matrix $\mathbf{P}$ of the estimation error

$$\mathbf{P}_{k|k-1} = \mathbf{F}_{k-1}\mathbf{P}_{k-1|k-1}{\mathbf{F}_{k-1}}^{\mathrm{T}} + \mathbf{Q}_{k-1} \tag{18}$$

and the estimation output error

$$\tilde{\mathbf{y}}_k = \mathbf{y}_k - g\left(\hat{\mathbf{x}}_{k|k-1}\right) \tag{19}$$

The innovation covariance matrix $\mathbf{S}$ and the near-optimal Kalman gain $\mathbf{K}$ are

$$\mathbf{S}_k = \mathbf{C}_k\mathbf{P}_{k|k-1}{\mathbf{C}_k}^{\mathrm{T}} + \mathbf{R}_k, \quad \mathbf{K}_k = \mathbf{P}_{k|k-1}{\mathbf{C}_k}^{\mathrm{T}}{\mathbf{S}_k}^{-1}. \tag{20}$$

The new state vector and covariance become

$$\hat{\mathbf{x}}_{k|k} = \hat{\mathbf{x}}_{k|k-1} + \mathbf{K}_k\tilde{\mathbf{y}}_k, \quad \mathbf{P}_{k|k} = \left(\mathbf{I} - \mathbf{K}_k\mathbf{C}_k\right)\mathbf{P}_{k|k-1}. \tag{21}$$

where $\mathbf{Q}$ and $\mathbf{R}$ are the covariance matrices of the process and observation noises, respectively.

In the presented implementation, the fast calculation time has been the priority, and therefore, the continuous-time nonlinear model (17) has been discretized using numerical integration and series expansion.

3 State Feedback Control

In order to test the EKF for different control methods, we implement the LQ state feedback control. The optimal feedback gain $\mathbf{L}$ is obtained by solving the minimization problem with the quadratic performance index J_q, that is,

$$J_q = \int_0^\infty \left[\mathbf{x}^{\mathrm{T}}\mathbf{Q}_r\mathbf{x} + \mathbf{u}^{\mathrm{T}}\mathbf{R}_r\mathbf{u}\right]dt, \tag{22}$$

where $\mathbf{Q}_r$, $\mathbf{R}_r$, and t are the state weighting matrix, the control input weight matrix of a regulator design, and time. To determine the diagonal weighting matrices $\mathbf{Q}_r$ and $\mathbf{R}_r$, we apply Bryson's rules [11]. The diagonal weighting coefficients are heuristically fine-tuned.

After implementing the filter, the estimation dynamics are selected. First, the matrices of process noise variance $\mathbf{Q}$ and the measurement noise variance $\mathbf{R}$ are selected similarly to the diagonal weighting matrices $\mathbf{Q}_r$ and $\mathbf{R}_r$.

Second, the **Q** and **R** are scaled by the common constant factor such that the steady-state linearized estimator dynamics are up to three times faster than the LQ regulator dynamics. The resulting closed-loop eigenvalues of the linearized steady state solutions are given in Appendix B.

4 Simulation Results

4.1 Current Controlled Bearings

First, the current controlled AMB balancing beam system is connected to the controller with state vector, which comprises the tilting angle and angular velocity. The regulator weighting matrices and the noise variance matrices are selected such as:

$$\mathbf{Q}_{\mathrm{r}} = diag\left\{1/(0.6\cdot\theta_0)^2,\quad 1/(0.1\cdot\dot{\theta}_0)^2\right\},\ \mathbf{R}_{\mathrm{r}} = diag\left\{1/(0.3\cdot i_{\max})^2,\quad 1/(0.3\cdot i_{\max})^2,\right\} \tag{23}$$

$$\mathbf{Q} = diag\left\{(\theta_0)^2,\quad (\dot{\theta}_0)^2\right\},\ \mathbf{R} = (0.01\cdot\theta_0)^2.$$

The cascaded controller is tested with the voltage plant model based on flux state variables. The closed-loop responses for the LQ regulator and the steady state linearized estimator are presented in Figure 2. The responses improve when the steady-state estimator is replaced with the EKF as shown in Figure 3.

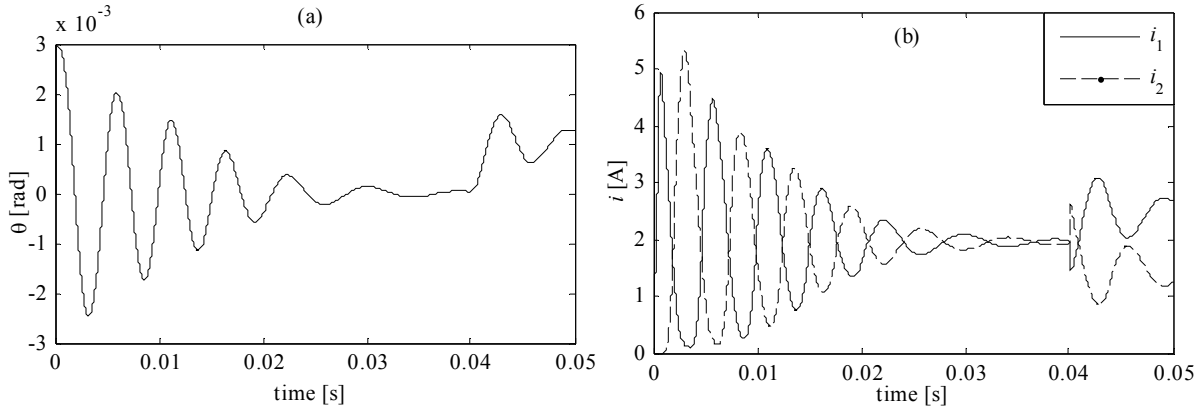

Figure 2: Closed-loop simulation of the lift up and step reference response when using steady-state linearized estimator: (a) tilting angle of the balancing beam and (b) coil currents

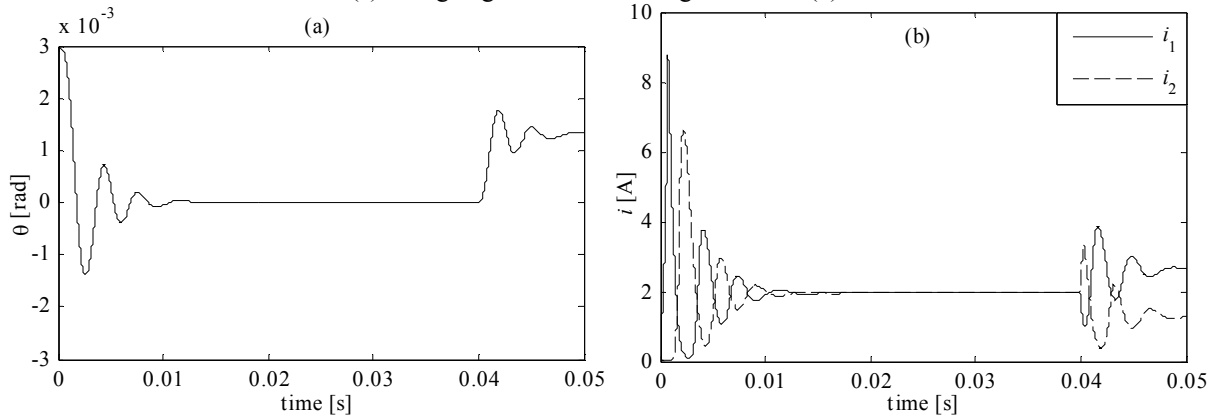

Figure 3: Closed-loop simulation of the lift up and step reference response when using EKF with modeled magnetic saturation: (a) tilting angle of the balancing beam and (b) coil currents

The closed-loop performance of the EKF based on saturation model improves slightly compared to the EKF based on classical analytical force model. When lifting the beam from $0.95\cdot\theta_0$ initial angle to $\theta = 0$, the resulting minimum angle before stabilizing at zero is -1.39 rad and -1.42 rad when using the model (4) and (5), respectively.

Second, the coil currents are added to the state vector in the controller employing (9). The order of the position outer controller increases from two to four. The regulator weighting matrices and the noise variance matrices are selected such as:

$$\mathbf{Q}_r = diag\left\{1/(0.6\cdot\theta_0)^2,\ 1/(0.1\cdot\dot{\theta}_0)^2,\ 1/(0.8\cdot i_{max})^2,\ 1/(0.8\cdot i_{max})^2\right\},\qquad \mathbf{R}_r = diag\left\{1/(0.3\cdot i_{max})^2,\ 1/(0.3\cdot i_{max})^2\right\},$$
$$\mathbf{Q} = diag\left\{(\theta_0)^2,\ (\dot{\theta}_0)^2,\ (100\cdot i_{max})^2,\ (100\cdot i_{max})^2\right\},\ \mathbf{R} = diag\left\{(0.01\cdot\theta_0)^2\ \ (100\cdot i_{max})^2\ \ (100\cdot i_{max})^2\right\} \quad (24)$$

The closed-loop responses for the LQ regulator and the steady-state linearized estimator are presented in Figure 4. The responses improve when the steady-state estimator is replaced with the EKF that includes magnetic and voltage saturation models as shown in Figure 5. When lifting the beam from $0.95\cdot\theta_0$ initial angle to $\theta = 0$, the resulting minimum angle before stabilizing at zero is -1.00 rad and -1.01 rad when using the model with the saturations and without, respectively. Evidently, the coil currents are such that the system is not deeply saturated. The discrete implementation of this controller required decreasing the sampling time from 20 μs to 4 μs.

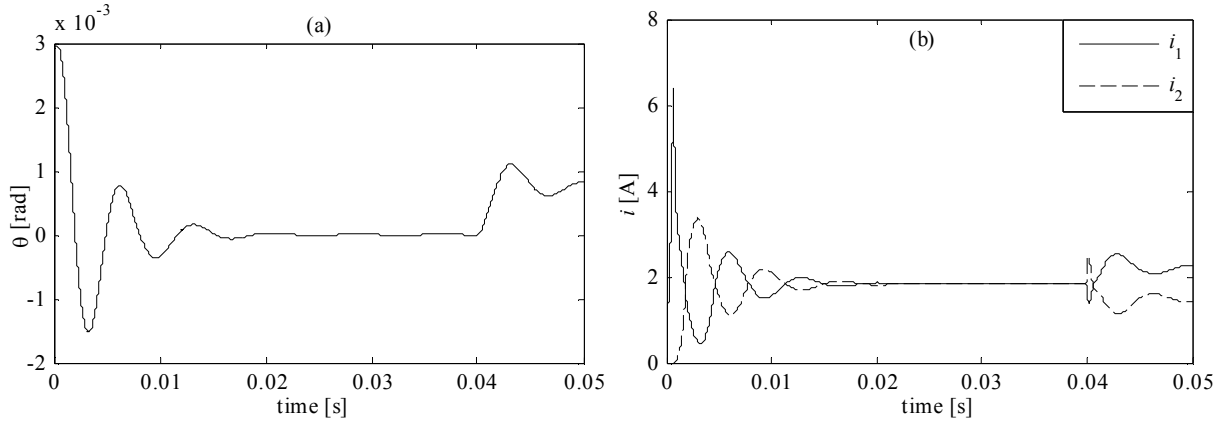

Figure 4: Closed-loop simulation of the lift up and step reference response when using steady-state linearized estimator: (a) tilting angle of the balancing beam and (b) coil currents

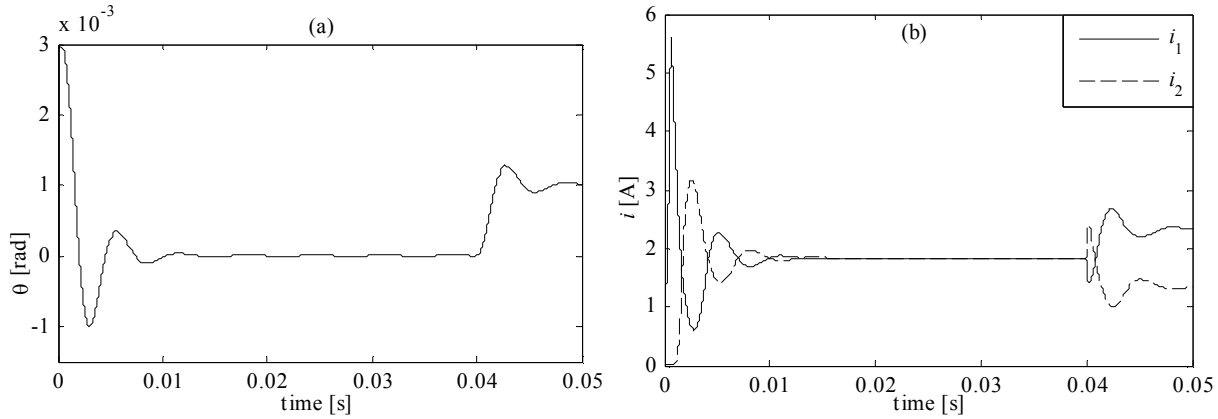

Figure 5: Closed-loop simulation of the lift up and step reference response when using EKF with modeled magnetic saturation and voltage saturation: (a) tilting angle of the balancing beam and (b) coil currents

4.2 Voltage Controlled Bearings

The voltage controlled AMB balancing beam system is connected to the non-cascaded controller. The regulator weighting matrices and the noise variance matrices are chosen the same as in the case of the more complex position controller (24) for current controlled AMB. However, the maximum current is replaced with the dc-link voltage in the control input weight matrix of a regulator design.

The closed-loop responses for the LQ regulator and the steady-state linearized estimator are presented in Figure 6. The responses improve when the steady-state estimator is replaced with the EKF as shown in Figure 7, even if the scaling matrices are not optimal. The closed-loop performance of the EKF based on saturation model improves marginally compared to the EKF based on classical analytical force model.

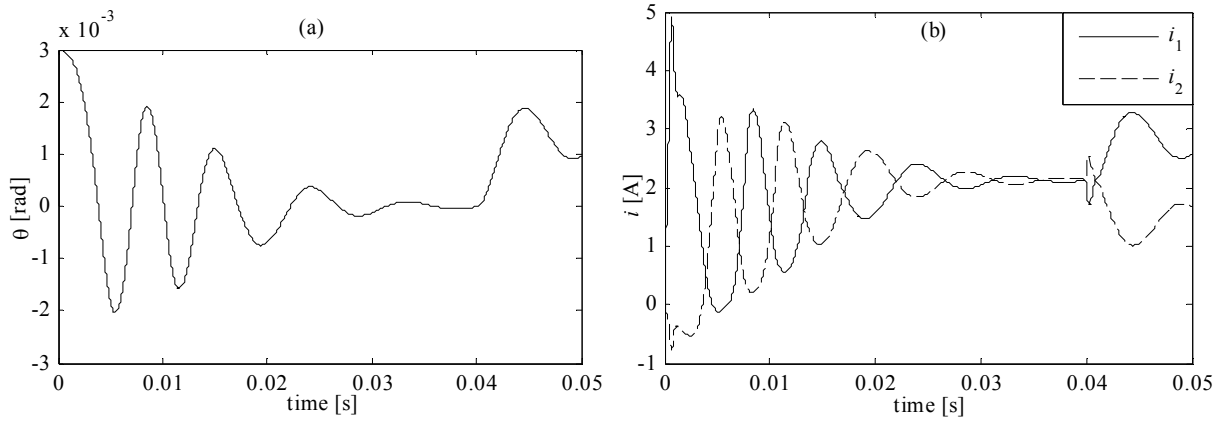

Figure 6: Closed-loop simulation of the lift up and step reference response when using steady-state linearized estimator: (a) tilting angle of the balancing beam and (b) coil currents

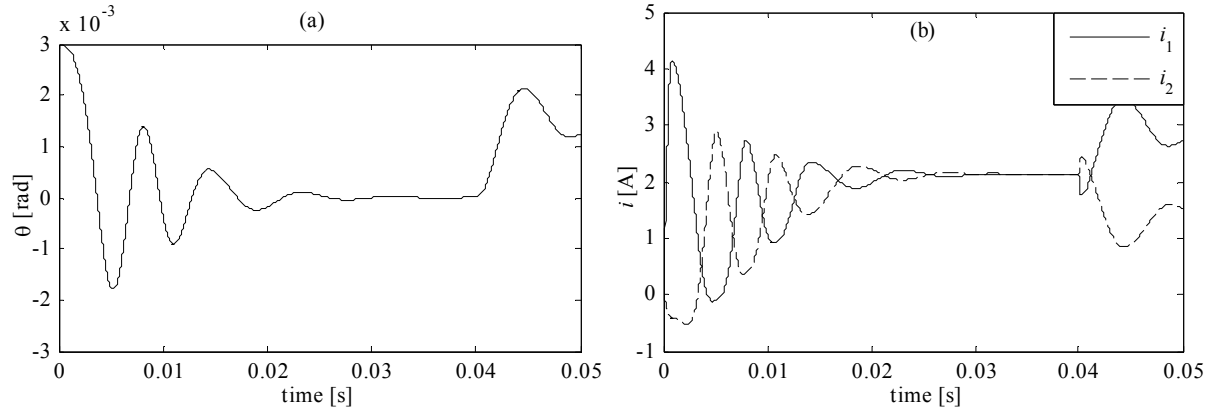

Figure 7: Closed-loop simulation of the lift up and step reference response when using EKF with modeled magnetic saturation: (a) tilting angle of the balancing beam and (b) coil currents

5 Conclusions

The work focused on the estimation of states for the AMB system with magnetic saturation and voltage saturation. It has been shown that including the EKF improves the state estimation and, consequently, any state feedback control for the presented current- and voltage-controlled AMBs. In the case of the current-controlled amplifiers, the EKF provides simple implementation if the amplifier dynamics are not modeled in the estimator. However, if the dynamics of the inner current control loops are included in the EKF implementation, the computational complexity is greater than in the case of the voltage-controlled AMBs. The voltage control based on fluxes or currents as the state variables are similarly suitable for the computationally efficient implementation of the EKF. Moreover, the voltage saturation does not have to be implemented when the voltage control is applied. In the case of the flux-

controlled AMBs, the inner control loop linearizes the magnetic force behavior leaving the implementation of the EKF with magnetic saturation questionable for the outer controller and complete plant dynamics.

Future work will focus on the experimental evaluation of the selected control configurations with the EKF. We plan to extend the proposed solution to more complex AMB rotor systems. The inclusion of hysteresis and eddy current models will be studied for some bearing structures. Additionally, the implementation of the EKF with the fluxed controlled AMBs and different regulator structures requires closer examination.

References

[1] H.W. Sorenson. *Kalman Filtering: Theory and Application*, IEEE Press, 1985.

[2] T. Schuhmann, W. Hofmann, R. Werner. Adaptive Linear and Extended KALMAN Filter Applied to AMB with Collocated Position Measuring, *ISMB10*, 2006.

[3] C.M. Zingerli and J.W. Kolar. Novel Observer Based Force Control for Active Magnetic Bearings, *IPEC*, pp. 2189–2196, 2010.

[4] H. Bleuler, D. Vischer, G. Schweitzer, A. Traxler and D. Zlatnik. New Concepts for Cost-effective Magnetic Bearing Control, *Automatica*, Vol. 30, No. 5: 871–876, 1994.

[5] T. Hu, Z. Lin, W. Jiang, P. E. Allaire. Constrained Control Design for Magnetic Bearing Systems, *Journal of Dynamic Systems, Measurement, and Control*, Vol. 127: 601–616, 2005.

[6] Y.N. Zhuravlyov. On LQ-Control of Magnetic Bearing, *IEEE Transactions On Control Systems Technology*, Vol. 8, No. 2: 344–350, 2000.

[7] G. Schweitzer, E.H. Maslen, Editors. *Magnetic Bearings: Theory, Design, and Application to Rotating Machinery*, Springer, New York, 2009.

[8] R.P. Jastrzebski1, A. Smirnov, O. Pyrhönen. Force Controllers for AMB Systems with Position and Current Feedback, *Solid State Phenomena*, accepted for publication, 2012.

[9] C.K. Chui and G. Chen. *Kalman Filtering With Real-Time Applications*. 3rd ed. Berlin, Germany: Springer-Verlag, 1999.

[10] T. Schuhmann, W. Hofmann, R. Werner. Improving Operational Performance of Active Magnetic Bearings Using Kalman Filter and State Feedback Control. *Transactions On Industrial Electronics*, Vol. 59, No. 2: 821–829, 2012.

[11] G.F. Franklin, J.D. Powell and M. Workman. *Digital control of dynamic systems*, 3rd edn. Addison-Wesley, Reading, 1998.

Appendix A

Parameter	Value	Parameter	Value	Parameter	Value
N	2·280	R	2 Ω	k_i	340 N/A
l_{Fe}	0.2 m	$i_{\max}$	10 A	k_x	1.36e6 N/m
S_{air}	1.08e-4 m^2	i_0	2 A	T_{s}	20 µs
r	0.16 m	u_{dc}	150 V	θ_0	0.0031 rad
l_0	5e-4 m	ω_{bw}	2000 rad/s	$\dot{\theta}_0$	383 rad/s
J	0.0093 kg·m^2	L	0.0426 H		

Table 1: Test rig parameters

Appendix B

Control configuration	Eigenvalue	Damping	Frequency
Current control, no actuator model in the position control loop	-2.39e+03 + 1.38e+03i	8.66e-01	2.76e+03
(regulator)	-2.39e+03 - 1.38e+03i	8.66e-01	2.76e+03
(estimator)	-2.88e+03 + 2.13e+03i	8.04e-01	3.58e+03
	-2.88e+03 - 2.13e+03i	8.04e-01	3.58e+03
Current control, actuator model in the position control loop	-2.40e+03	1.00e+00	2.40e+03
(regulator)	-1.73e+03 + 1.87e+03i	6.79e-01	2.55e+03
	-1.73e+03 - 1.87e+03i	6.79e-01	2.55e+03
	-2.18e+03	1.00e+00	2.18e+03
(estimator)	-2.78e+03 + 2.63e+03i	7.27e-01	3.83e+03
	-2.78e+03 - 2.63e+03i	7.27e-01	3.83e+03
	-5.25e+03	1.00e+00	5.25e+03
	-5.40e+03	1.00e+00	5.40e+03
Voltage control	-1.33e+03	1.00e+00	1.33e+03
(regulator)	-6.81e+02 + 1.16e+03i	5.08e-01	1.34e+03
	-6.81e+02 - 1.16e+03i	5.08e-01	1.34e+03
	-1.40e+02	1.00e+00	1.40e+02
(estimator)	-2.75e+03 + 2.74e+03i	7.07e-01	3.88e+03
	-2.75e+03 - 2.74e+03i	7.07e-01	3.88e+03
	-5.00e+03	1.00e+00	5.00e+03
	-5.00e+03	1.00e+00	5.00e+03

Table 2: Closed-loop characteristics of tested control configurations